ELSEVIER

Contents lists available at ScienceDirect

# Geochimica et Cosmochimica Acta

journal homepage: www.elsevier.com/locate/gca





# Potassium-39-derived $^{36}$ Ar production during fission-neutron irradiation and its effect on $^{40}$ Ar/ $^{39}$ Ar ages

Jack N. Carter a,b,\*, Paul R. Renne b, Leah E. Morgan

- <sup>a</sup> Berkeley Geochronology Center, 2455 Ridge Rd, Berkeley, CA 94709, USA
- <sup>b</sup> Department of Earth and Planetary Science, University of California Berkeley, Berkeley, CA 94720, USA
- <sup>c</sup> U.S. Geological Survey, Denver Federal Center, MS 963, Denver, CO 80225, USA

# ARTICLE INFO

Associate editor: Janne Blichert-Toft

Keywords: <sup>40</sup>Ar/<sup>39</sup>Ar geochronology Neutron irradiation Interferences Nuclei production Intercalibration

# ABSTRACT

Various interference reactions producing unwanted Ar isotopes from K, Ca, Cl and Ar require correction to satisfy the  $^{40}\text{Ar}/^{39}\text{Ar}$  age equation. Using GEANT4, we design and build a model Cadmium Lined In Core Irradiation Tube (CLICIT) irradiation facility, as used in the Oregon State TRIGA Reactor (OSTR). We illustrate the complexity of the irradiation of geologic samples within this framework and determine an overlooked production channel of  $^{36}\text{Ar}$ . The production of  $^{36}\text{Ar}$  is fed from the  $^{39}\text{K}(n,\alpha)^{36}\text{Cl}$  nuclear channel,  $^{36}\text{Cl}$  subsequently decays to  $^{36}\text{Ar}$  ( $^{39}\text{K}(n,\alpha,\beta)$ )  $^{36}\text{Ar}$ ). Simulations in this work using a  $^{235}\text{U}$  fission neutron energy spectrum and modelled CLICIT facility, determine a production ratio for this reaction ( $^{36}\text{Cl}/^{39}\text{Ar})_{\text{K}} = 0.40 \pm 0.01$  ( $^{1}\sigma$ ); greater than an order of magnitude larger than any other K interference. The magnitude of the resulting age bias for an unknown sample will be a function of the integrated neutron flux, the length of irradiation (fluence), the time elapsed since irradiation, and the age relationship between the unknown and neutron fluence monitor. We show using the raw data of (Niespolo et al., 2017) that the age of Alder Creek sanidine can be modified to be ca. 0.1% older ( $^{1}\sigma$ ), at the 2 $^{1}\sigma$  level of current analytical precision for the Alder Creek age for this study. The  $^{39}\text{K}(n,\alpha,\beta)^{36}\text{Ar}$  inference should be incorporated into routine data analysis and may be especially important in the intercalibration of the  $^{40}\text{Ar}/^{39}\text{Ar}$  system with other chronometers (e.g.,  $^{206}\text{Pb}/^{238}\text{U}$ ).

# 1. Introduction

The  $^{40}\text{Ar}/^{39}\text{Ar}$  technique (Merrihue and Turner, 1966) is a versatile dating method in terms of application to a range of geologic timescales and settings.  $^{40}\text{Ar}/^{39}\text{Ar}$  dating is based on the potassium-argon (K-Ar) dating method, where the K content of the sample is calibrated to the  $^{39}\text{Ar}$  produced from the  $^{39}\text{K}(n,p)^{39}\text{Ar}$  nuclear channel during irradiation. To determine the production of  $^{39}\text{Ar}$  from  $^{39}\text{K}$  ( $^{39}\text{Ar}_\text{K}$ ) in the sample of interest (which is termed the unknown), it is necessary to co-irradiate it with another material. This other material, which has a precisely and independently known age or  $^{40}\text{Ar}*/^{39}\text{Ar}_\text{K}$  ratio, is referred to as the neutron fluence monitor. Following irradiation, the relative abundances of the parent proxy  $^{39}\text{Ar}$  ( $^{39}\text{Ar}_\text{K}$ ) and the radiogenic daughter  $^{40}\text{Ar}$  can be measured by mass-spectrometry of both the unknown and neutron fluence monitor to satisfy the  $^{40}\text{Ar}/^{39}\text{Ar}$  age equation. Typically, samples are irradiated using  $^{235}\text{U}$  fission neutrons (Watt spectrum; Watt, 1952). Fig. 1 shows how the necessary  $^{39}\text{K}(n,p)^{39}\text{Ar}$  reaction cross-section (Evaluated Nuclear Data File (ENDF)/N-VIII.0 database; Brown

et al. 2018) varies across the Watt fission spectrum of neutron energies ranging from 0 to 20 MeV. Also shown in Fig. 1 are recent measurements by Rutte et al. (2019) of the cross-section using neutrons from a Deuterium-Deuterium fusion (High Flux Neutron Generator (HFNG)) and  $^7\text{Li}(p,n)$   $^7\text{Be}$  (Lithium Inverse Cinematic ORsay Neutron source (LICORNE)) sources with incident neutron energies ranging from ca. 1 to 3 MeV. We also demonstrate the interaction cross-sections of additional argon production pathways from K and Ca, within the scope of fission neutron energies. These are shown in Fig. S1.

Recent methodological developments including (1) New generation of multi-collector noble gas mass spectrometers (e.g., Phillips and Matchan, 2013; Mixon et al., 2022), (2) Increased attention to precise determination of the neutron fluence, and (3) the use of independently calibrated neutron fluence monitor ages (e.g., Kuiper et al., 2008). These improvements in the  $^{40}$ Ar/ $^{39}$ Ar technique have now made it possible to ascertain ages with an analytical precision of 0.05%, as reported by Niespolo et al. (2017). This level of precision was determined based on the weighted mean and the associated uncertainty derived from all the

E-mail address: jcarter@bgc.org (J.N. Carter).

<sup>\*</sup> Corresponding author.

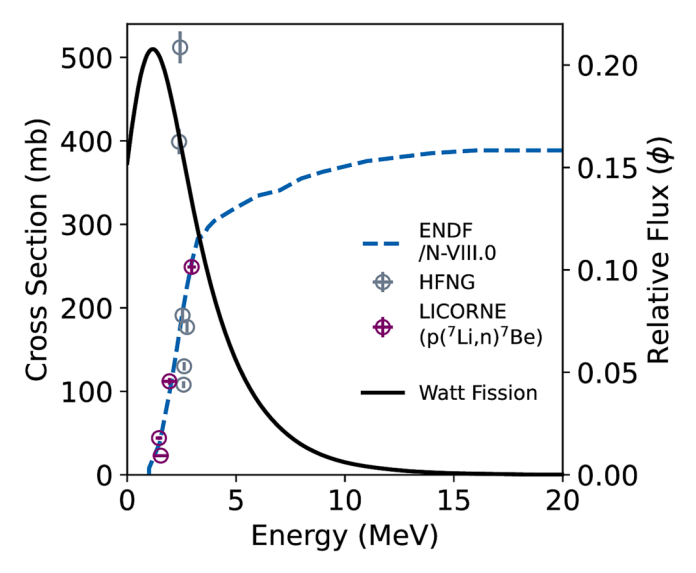


**Fig. 1.** This Fig. Shows the Watt fission spectrum that describes the distribution of neutron energies released during the fission process (black line). The cross-section of the  $^{39}$ K(n,p) $^{39}$ Ar interaction is shown as a dashed blue line and the data is taken from collection of nuclear data libraries that are compiled in the Evaluated Nuclear Data File (ENDF) VIII.0 database. Rutte et al. (2019) D-D measurements in gray and  $^{7}$ Li(p,n) $^{7}$ Be shown in purple. It can be seen directly from these measurements that the cross-section has more complex structure in the 1–3 MeV range than compared to the smooth cross-section of the ENDF VIII.0 database (Brown et al. 2018).

analyses performed by Niespolo et al. (2017). With this improved precision, sources of uncertainty that were previously considered to be negligible require re-assessment. Foremost among these are the decay constants of <sup>40</sup>K, which are the subject of ongoing investigations (Hariasz et al., 2022); Stukel et al., 2022) but are not considered here. Another category of uncertainties is rooted in the required neutron irradiation of samples and can be grouped as follows; (1) Recoil of <sup>37</sup>Ar and <sup>39</sup>Ar (e.g., Turner and Cadogan, 1974; Onstott et al. 1995; Villa, 1997; Renne et al., 2005; Jourdan et al., 2007; Hall, 2014; Paine et al., 2006); (2) Neutron fluence gradients (e.g., Rutte et al., 2015) and; (3) Interference channels (e.g., Turner, 1971; Dalrymple and Lanphere, 1971).

The energy spectrum of <sup>235</sup>U fission neutrons results in the production of a suite of unwanted argon isotopes (spanning the most important atomic mass units 36-40) by various nuclear production channels. These reactions are in addition to the desired <sup>39</sup>K(n,p)<sup>39</sup>Ar reaction and result from nuclear processes on the nuclei of samples whose chemical and isotopic compositions (i.e., concentrations of nucleons) vary widely. Production pathways are dominated by reactions on isotopes of potassium and calcium (Fig. S1) with less probable channels on isotopes of chlorine and argon. These additional nucleogenic sources of argon are known as interferences. To account for these interferences and to correctly satisfy the <sup>40</sup>Ar/<sup>39</sup>Ar age equation requires the measurement of the Ar isotopes ranging in atomic mass units from 36 to 40 (e.g., Mitchell, 1968; Brereton, 1970; Turner, 1971; Dalrymple, 1981; McDougall and Harrison, 1999; Renne et al. 2005). Table 1 shows the argon isotope production pathways that are most important for <sup>40</sup>Ar/<sup>39</sup>Ar dating; including channels that have been previously determined (e.g., Turner, 1971; Renne et al., 2010) and from the simulations in this work using GEANT4 which uses the ENDF V-III.0 database. Fig. S1 panels A and B show the ENDF V-III.0 (Brown et al. 2018) nuclear database cross-sections for Ar production nuclear channels from isotopes of K and Ca as a function of incident neutron energy. The importance of these corrections depends on the sample composition and age, and flux and profile of the neutron energy spectrum, the duration of the irradiation (neutron fluence), and the elapsed time between irradiation

Table 1
Nuclear channels for the production of Ar isotopes from Ca, K, Ar, and Cl.

Isotope produced	Ca	K	Ar	Cl
<sup>36</sup> Ar	$^{40}$ Ca(n,n) $^{1,2,3}$	$^{39}$ K(n, $\alpha$ , $\beta$ ) $^{1,*}$		<sup>35</sup> Cl(n,γ, β) <sup>1,2,*</sup>
<sup>37</sup> Ar	$^{40}$ Ca $(n,\alpha)^{1,2,3,}$	$^{39}$ K(n,t) $^{1,2,*}$	$^{36}$ Ar(n, $\gamma$ ) <sup>1,2,</sup>	
<sup>38</sup> Ar <sup>39</sup> Ar	<sup>40</sup> Ca(n, <sup>3</sup> He)* <sup>41</sup> Ca(n,)* <sup>42</sup> Ca(n,n) <sup>1,2,3</sup> , * <sup>43</sup> Ca(n,2n)* <sup>40</sup> Ca(n,2p)* <sup>42</sup> Ca(n,α) <sup>1,2,3</sup> ,	$^{39}$ K(n, $^{19}$ ) $^{1,2,3*}$ $^{40}$ K(n,t)* $^{41}$ K(n, $\alpha$ , $\beta$ ) $^{1,3}$ , * $^{39}$ K(n,p) $^{1,2,*}$ $^{40}$ K(n,np) $^{1,2,*}$	$^{40}$ Ar(n,t,) <sup>1,2,</sup> * $^{38}$ Ar(n, $\gamma$ ) <sup>1,2,</sup> * $^{40}$ Ar(n,	<sup>37</sup> Cl(n,γ, β 1,2, <sub>±</sub>
<sup>40</sup> Ar	$^{43}$ Ca(n, $n\alpha$ ) $^{1,2,3,*}$ $^{42}$ Ca(n, $^{3}$ He) $^{*}$ $^{43}$ Ca(n, $\alpha$ ) $^{1,2,*}$ $^{44}$ Ca(n, $n\alpha$ ) $^{1,2,*}$	$^{41}$ K(n,t)* $^{40}$ K(n,p) <sup>1,2,*</sup> $^{41}$ K(n, np) <sup>1,2,*</sup>	d,) <sup>1,2,*</sup> <sup>40</sup> Ar(n,2n)*	

<sup>\*</sup> Simulation (This study).

and measurement. Due to this dependence on the energy profile and flux, the suite of interferences applied for a given unknown and neutron fluence monitor will be unique to each reactor, and position within the reactor, used for the irradiation.

The majority of relevant corrections for interfering reactions on K and Ca have been well established for the suite of nuclear reactors used for  $^{40} \rm Ar/^{39} Ar$  dating. The optimal way to determine interference corrections is to measure the produced argon isotopes in samples of pure Ca and K materials irradiated under identical conditions as unknowns and neutron fluence monitors. Relevant production ratios are then calculated and are used to correct the unknown and neutron fluence monitor materials.

Nuclear channels have a strong energy dependence; therefore, additional mechanisms can also be used to limit the production pathway of certain argon isotopes. One example is the  $^{40}$ K(n,p) $^{40}$ Ar nuclear channel. The cross-section of this reaction is particularly dominant in the thermal part of the neutron energy spectrum, i.e., <0.025 eV. The production of  $^{40}$ Ar by this channel can be significantly reduced by shielding with a strong thermal neutron absorber, such as cadmium (Tetley et al., 1980). By diligent choice of irradiation time and shielding, interferences can be minimized and the introduced errors can be kept below 1% (e.g., Dalrymple and Lanphere, 1971; Renne et al., 2005). However, for extreme cases such as young samples with low K/Ca ratios, interference reactions (particularly from calcium) can be the ultimate accuracy-limiting factor.

The purpose of this work is to assess the irradiation process for both routinely analyzed sample types and materials used for interference corrections in  $^{40} \rm Ar/^{39} Ar$  geochronology. We simulate the irradiation process with particular emphasis on Ar-producing nuclear channels, we demonstrate the intricate nature of irradiation and showcase the variety of nuclei and particles generated in geological samples during this process. The significance of the often-overlooked  $^{39} \rm K(n,\alpha,\beta)^{36} Ar$  channel is emphasized, along with the argon correction equations necessary for determining the  $^{40} \rm Ar^*$  and  $^{39} \rm Ar_K$  from all measured argon isotopes, taking this interference into account. Argon correction equations are given in the supplementary material.

# 2. Methods

GEANT4 is an open-source software toolkit for simulating the passage of particles through matter (Agostinelli et al., 2003). Applications

<sup>&</sup>lt;sup>1</sup> Renne et al., (2005).

<sup>&</sup>lt;sup>2</sup> Brereton (1970).

<sup>&</sup>lt;sup>3</sup> Turner (1971).

range from particle physics to space engineering and medical physics in the particle energy range of eV to TeV. In this work, GEANT4 Monte Carlo models (version 4.10.07.p02) have been built to simulate the irradiation process in the Cadmium Lined In Core Irradiation Tube (CLICIT) at the Oregon State TRIGA Reactor (OSTR), the most widely used reactor for <sup>40</sup>Ar/<sup>39</sup>Ar dating (Rutte et al., 2018). The ENDF.VIII.0 cross-section database is used for all simulations. We compare the results of these simulations to data recorded in Renne et al. (2005) and document nuclear processes. All GEANT4 simulation code can be found here https://github.com/jcarter-1/Nucleogenic\_36Ar and all datasets and analytical methods can be found here https://doi.org/10.6084/m9.figsh are.22126607.

### 3. Irradiation of geological samples

In this section we present a summary of neutron irradiation with geologic samples with focus on the current suite of interference corrections used in  $^{40}$ Ar $/^{39}$ Ar geochronology.

# 3.1. Interaction of neutrons with geologic samples

As well as the desired production of  $^{39} Ar_K$ , the interaction of neutrons with geologic samples will produce a suite of argon isotopes ranging in atomic mass units from 36 to 40. In addition to the production of argon, interaction of neutrons with all of the compositional isotopes within the sample will have produced an array of isotopes and particles. To illustrate the complexity of this process we simulate the irradiation of an ideal (no impurities) 250  $\mu m$  K-feldspar type sample (composition; Fig. S2) with 5  $\times$  108 prompt fission neutrons. All nuclei that that are both formed or undergo scattering reactions are shown in Fig. 2. An identical plot for a hornblende type sample (composition Fig. S3) is given in the supplement (Fig. S4).

The creation of charged free particles during irradiation such as alphas or protons have the potential to form helium or hydrogen which could potentially interfere with the ion-optics of the mass spectrometer. The production of hydrogen from the  $^{39}\text{K(n,p)}^{39}\text{Ar}$  reaction, where the proton p is a + 1 hydrogen ion, can potentially lead to the formation of molecules, such as  $\text{H}^{35}\text{Cl}$ , by combining with chlorine. This process results in a mass-to-charge (m/e) ratio that is identical to that of the  $^{36}\text{Ar}$  isotope, which can subsequently cause mass interferences in the analysis. This isobar would require a mass spectrometer with a high resolving power to resolve it from  $^{36}\text{Ar}$ . Phillips et al. (2017) determine that a resolving power of 8000 is required to separate the two masses. We do not directly model this, but highlight it as another source of complexity in the irradiation of geologic samples.

Secondary processes involving the ejected daughter particles can occur, for example the ejected proton can initiate the  $^{40}{\rm Ar}(p,n)^{40}{\rm K}$  reaction which has a peak cross-section at  ${\sim}800$  millibarns for an incident 10 MeV proton (relative to 400 millibarns at ca. 20 MeV for the  $^{39}{\rm K}(n,p)^{39}{\rm Ar}$  reaction channel) (ENDF database; Brown et al., 2018). To our knowledge these secondary processes have not been discussed in the literature, but with ever increasing precision of analytical data may require revisiting.

Another important process is the production of gamma particles ( $\gamma$ ).  $\gamma$ 

particles are produced by  $(n,\gamma)$  reactions and the de-excitation of nuclei during irradiation. Following production, these  $\gamma$  particles can interact with the sample which is the primary mechanism by which samples are heated during an irradiation. Typically, samples undergoing irradiations reach temperatures of approximately 200 °C which has the potential to cause some thermally activated loss of argon in samples which have a lower retention of argon, such as illite (e.g., Clauer et al., 2012).

### 3.2. Interference corrections

The suite of argon isotopes produced (aside from the desired  $^{39}{\rm Ar_K}$ ) during irradiation require corrections to satisfy the age equation. These produced isotopes are generally unwanted and propagate uncertainty into a calculated age. However, some can be useful chemical tracers such as  $^{37}{\rm Ar}$  for calcium or  $^{38}{\rm Ar}$  for chlorine. The formation rate of these, and all activation products, is given by:

$$R_n = \phi(E)n\sigma(E) \tag{1}$$

where  $R_n$  is the rate of formation (Number of formed nuclei per second),  $\phi(E)$  is the flux (neutrons/cm<sup>2</sup>/s), n is the number of target nucleons, and  $\sigma(E)$  is the cross-section of the interaction (barns (1 × 10<sup>-24</sup> cm<sup>2</sup>)). Note that both the flux and cross-section of Eq. (1) are energy dependent and thus will be unique for a given reactor and position of the sample within the reactor. Knowledge of the amount of produced interference argon isotopes is required to apply the <sup>40</sup>Ar/<sup>39</sup>Ar age equation correctly. Interference corrections are formatted as follows (XAr/YAr), where X is the interference isotope, Y is the primary/desired isotope which the interference is measured relative to, and Z is the target element (e.g., K). For example, the  $(^{38}\text{Ar}/^{39}\text{Ar})_{\text{K}}$  ratio designates the  $^{38}\text{Ar}/^{39}\text{Ar}$  ratio produced from all isotopes of K. Shown in Table 1, the production channels of  ${}^{38}$ Ar are:  ${}^{39}$ K(n,np)  ${}^{38}$ Ar,  ${}^{40}$ K(n,t)  ${}^{38}$ Ar,  ${}^{41}$ K(n, $\alpha$ ,  $\beta$ )  ${}^{38}$ Ar. For  ${}^{39}$ Ar the production channels from K are: <sup>39</sup>K(n,p)<sup>39</sup>Ar, <sup>40</sup>K(n,np)<sup>39</sup>Ar, and <sup>41</sup>K(n, t)<sup>39</sup>Ar. This is carried out for all interference channels to determine the  $^{40}$ Ar\* and  $^{39}$ Ar<sub>K</sub> and satisfy the  $^{40}$ Ar/ $^{39}$ Ar age equation which is given by

$$t = \frac{1}{\lambda} \left( 1 + J \left( \frac{^{40}Ar^*}{^{39}Ar_K} \right) \right) \tag{2}$$

where  $^{39}Ar_K$  is the  $^{39}Ar$  produced by  $^{39}K(n,p)^{39}Ar,\,^{40}Ar^*$  is the radiogenic portion of the total  $^{40}Ar$  measured,  $\lambda$  is the total decay constant, and J is the measure of neutron fluence determined by the analysis of a co-irradiated neutron fluence monitor of an independently determined age. J is given by:

$$J = \frac{e^{\lambda t_s} - 1}{\left(\frac{40}{30}Ar^{\circ}\right)_{S}} \tag{3}$$

where  $(^{40}\text{Ar*}/^{39}\text{Ar}_K)_S$  is the ratio of the radiogenic  $^{40}\text{Ar}$  to  $^{39}\text{Ar}_K$  in the neutron fluence monitor material,  $\lambda$  is the total decay constant, and  $t_s$  is the known age of the neutron fluence monitor. Interference corrections are required to determine the {\it true}  $^{40}\text{Ar*}$  and  $^{39}\text{Ar}_K$  of both the unknown sample and monitor material from the measured argon isotopes ranging from 36 to 40 in atomic mass units.

In most cases, the interference reactions on K and Ca (Fig. S1) are the

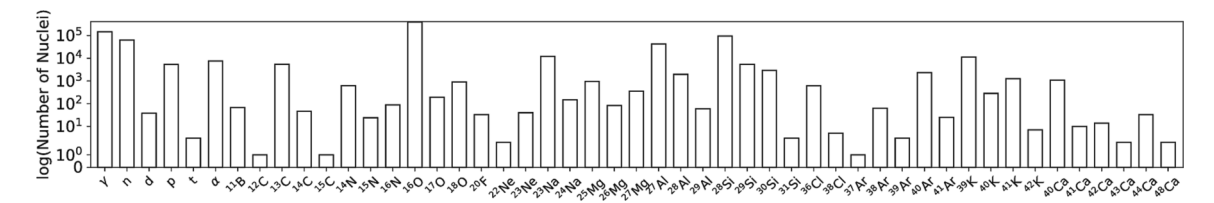


Fig. 2. Generated and scattered nuclei and particles from the irradiation of a 250  $\mu$ m feldspar type sample in the Cadmium Lined in Core Irradiation Tube (CLICIT). This irradiation consists of  $5 \times 10^8$  prompt fission neutrons. Nuclei shown are either formed or scattered by an interaction with a neutron. Natural nuclei (e.g., atmospheric Ar, that are not nucleogenic or have not been part of a scattering reaction) are not shown in the plot.

most relevant to the determination of a geologically meaningful age (i. e.,  $^{40}$ K(n,p) $^{40}$ Ar,  $^{40}$ Ca(n, $\alpha$ ) $^{37}$ Ar, and  $^{42}$ Ca(n,n $\alpha$ ) $^{39}$ Ar). Corrections for interferences have been well established by irradiating high-purity K and Ca materials under identical conditions to the <sup>40</sup>Ar/<sup>39</sup>Ar dating process (e.g., Brereton, 1970; Turner, 1971; Dalrymple and Lanphere, 1971; McDougall and Roksandic, 1974; Tetley et al., 1980; Roddick, 1983; Renne et al., 2005). As well as the dominant interferences on K and Ca, other argon isotope production channels on Cl, although relatively minimal in most situations, are not as well studied (Renne et al., 2008). Chlorine has two naturally occurring isotopes (<sup>35</sup>Cl and <sup>37</sup>Cl) which produce  $^{36}Cl$  and  $^{38}Cl$  by radiative capture, (n, $\gamma$ ), reactions and then both decay via beta emission to form both <sup>36</sup>Ar and <sup>38</sup>Ar. The short half-life of  $^{38}$ Cl ( $t_{1/2} \sim 37$  mins) ensures that essentially all  $^{38}$ Cl will have decayed to <sup>38</sup>Ar by the time of analyses. Unlike the decay of <sup>38</sup>Cl to <sup>38</sup>Ar,  $^{36}$ Cl decay to  $^{36}$ Ar has a much longer half-life ( $t_{1/2} \sim 3 \times 10^5$  a) meaning that this production channel to <sup>36</sup>Ar is most important for Cl-rich samples (Renne et al., 2008). Renne et al. (2008) construct the methodology for the correction of Cl-derived Ar isotopes and effects of these corrections on the apparent <sup>40</sup>Ar/<sup>39</sup>Ar age of a sample.

### 4. Results

In this section we present the currently overlooked  $^{39}\text{K}(n,\alpha,\beta)$   $^{36}\text{Ar}$  interference channel and determined the effect of this interference on  $^{40}\text{Ar}/^{39}\text{Ar}$  ages. Uncertainties are given at the 68% confidence interval throughout.

# 4.1. Overlooked nuclear production channel and age correction

The interfering reactions that create  $^{36}$ Ar are the most critical as  $^{36}$ Ar is used to determine the amount of atmospheric Ar in the sample and subsequently the atmospheric  $^{40}$ Ar budget. Atmospheric  $^{40}$ Ar is then then subtracted from the total  $^{40}$ Ar following all other interference corrections to determine the radiogenic  $^{40}$ Ar\*. Consequently, additional channels that add  $^{36}$ Ar to the system become particularly important. From the simulation of an irradiation for a 250  $\mu$ m K-feldspar composition sample we identify an additional production pathway of  $^{36}$ Ar ( $^{39}$ K ( $n,\alpha,\beta$ )  $^{36}$ Ar). We show all argon producing nuclear channels for the simulated irradiation of the 250  $\mu$ m feldspar sample in Fig. S5. In the next section we present corrections for the  $^{39}$ K( $n,\alpha,\beta$ )  $^{36}$ Ar nuclear channel and discuss the wider implications of this reaction for the determination of apparent  $^{40}$ Ar/ $^{39}$ Ar ages.

# 4.2. Corrections for overlooked $^{39}K(n,\alpha,\beta)$ $^{36}Ar$ nuclear channel

To illustrate the effect on an apparent 40Ar/39Ar age with the

inclusion of the  $^{39}$ K(n, $\alpha$ ,  $\beta$ )  $^{36}$ Ar interference, we use the raw data of Alder Creek sanidine and reference monitors used by Niespolo et al. (2017) and include the  $^{39}$ K(n, $\alpha$ ,  $\beta$ )  $^{36}$ Ar from the simulated irradiations. This correction will follow a similar framework to the chlorine correction formulated by Renne et al. (2008). To determine the  $^{39}$ K(n, $\alpha$ , $\beta$ )  $^{36}$ Ar interference correction we begin with the initial (<sup>36</sup>Cl/<sup>39</sup>Ar)<sub>K</sub> production ratio and then determine the (<sup>36</sup>Ar/<sup>39</sup>Ar)<sub>K</sub> correction from the ingrowth of <sup>36</sup>Ar from <sup>36</sup>Cl and decay of <sup>39</sup>Ar for a given time since irradiation  $(\Delta t_{\rm irr})$ . Similar to other interference corrections (e.g.,  $(^{36}Ar/^{37}Ar)_{\rm Ca})$  this ratio will be dependent only on the cross-section and will therefore be constant for a given irradiation. We initially create an Alder Creek type sample and perform six simulated irradiations in GEANT4 each with 1 imes10<sup>9</sup> incident fission neutrons (estimated to be 0.0002 MW/hr assuming that the OSU TRIGA reactor is operating at full power). We then determine an  $(^{36}Ar/^{39}Ar)_K$  interference correction by initially calculating the  $(^{36}\text{Cl}/^{39}\text{Ar})_{\text{K}}$  ratio which has a weighted mean and uncertainty of 0.40  $\pm$  $0.01 (1\sigma)$  (Fig. 3A). Following this we now present the relative corrections for the  $^{39}$ K(n, $\alpha$ , $\beta$ )  $^{36}$ Ar interference as a function of the time since irradiation ( $\Delta t_{irr}$ ) and then include this correction in the determination of the Alder Creek age using the data of Niespolo et al., (2017). The amount of <sup>36</sup>Ar derived from <sup>36</sup>Cl is given by:

$$^{36}Ar_{Cl} = ^{39}Cl_0(1 - e^{-\lambda_{36}\Delta t_{irr}})$$
 (4)

and the <sup>39</sup>Ar decay is given by:

$$^{39}Ar = ^{39}Ar_0(e^{-\lambda_{39}\Delta t_{irr}}) \tag{5}$$

where  $\Delta t_{irr}$  is the time elapsed between irradiation and analysis,  $\lambda_{36}$  and  $\lambda_{39}$  are the decay constants of  $^{36}\text{Cl}$  and  $^{39}\text{Ar}$ , and  $^{36}\text{Cl}_0$  and  $^{39}\text{Ar}_0$  are the initial values of  $^{36}\text{Cl}$  and  $^{39}\text{Ar}$  produced by the  $^{39}\text{K}(n,\alpha,\beta)$   $^{36}\text{Ar}$  and  $^{39}\text{K}(n,\rho)$   $^{39}\text{Ar}$  nuclear channels. The initial ratio ( $^{36}\text{Cl}_0/^{36}\text{Ar}_0$ ) is determined from the simulated irradiation and is 0.40  $\pm$  0.01. The ingrowth/decay curve is then calculated by the ratio of Eqs. (4) and (5):

$$\left(\frac{^{36}Ar}{^{39}Ar}\right)_{K} = \left(\frac{^{36}Cl_{0}}{^{39}Ar_{0}}\right) \frac{(1 - e^{-\lambda_{36}\Delta t_{irr}})}{(e^{-\lambda_{39}\Delta t_{irr}})}$$
(6)

Fig. 3B shows how the  $(^{36}\text{Ar}/^{39}\text{Ar})_K$  ratio evolves for a given  $\Delta t_{irr}$ . We use a Monte Carlo simulation to generate a 68% credible interval for the ingrowth/decay curve using the weighted mean and error of the initial  $(^{36}\text{Cl}/^{39}\text{Ar})_K$  ratio and decay constant uncertainties for both  $^{36}\text{Cl}$  and  $^{39}\text{Ar}$ . Decay constants and decay constant uncertainties of  $^{36}\text{Cl}$  and  $^{39}\text{Ar}$  are given in Table S1.

We use the simulated  $(^{36}\text{Ar}/^{39}\text{Ar})_K$  ratio (Fig. 3A) to estimate the change in age for the Alder Creek sanidine measured by Niespolo et al., (2017). In the study of Niespolo et al., (2017) the age of Alder Creek sanidine age is calibrated to astronomically dated Miocene tuffs. We re-

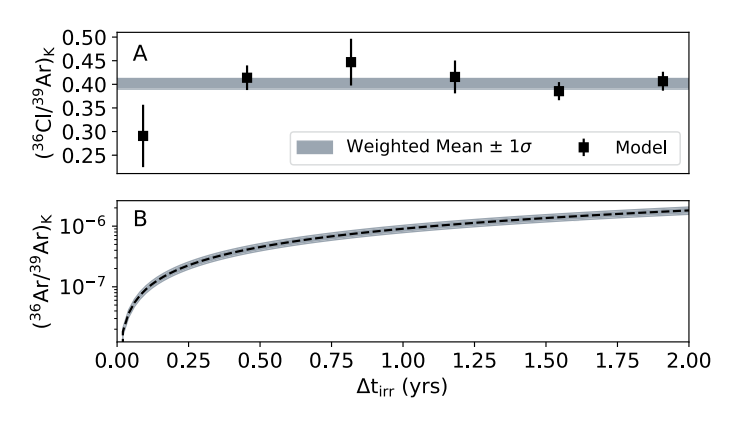


Fig. 3. Panel A shows the production of  $^{36}$ Cl relative to  $^{39}$ Ar derived from  $^{39}$ K. These ratios assume no decay in each formed isotope and error bars on the individual batch runs are only from counting statistic; N, where N is the number of generated atoms. The weighted mean and weighted mean error is also plotted (blue shaded bar) and is determined to be  $0.40 \pm 0.01$  ( $1\sigma$ ). Panel B shows magnitude of the Cl-correction as a function of time since irradiation. Initial values are determined by the weighted mean and weighted mean error of the formed number of atoms for each batch run. Uncertainty envelope shown is at the 68% credible interval.

determine the age of Alder Creek sanidine including the (<sup>36</sup>Ar/<sup>39</sup>Ar)<sub>K</sub> interference in the data reduction with each of the astro-chronological ages used as monitor materials; Mes4, FCs, and A1 (Kuiper et al., 2004; Kuiper et al., 2008; Rivera et al., 2011). The age correction is carried out as follows; the  $^{39}$ K(n, $\alpha$ ,  $\beta$ )  $^{36}$ Ar contribution to the  $^{36}$ Ar budget is determined assuming a  $\Delta t_{irr}$  of 3 months (Fig. 3B) and using the measured <sup>39</sup>Ar<sub>K</sub>, this is then subtracted from the total budget which is then used to determine the  $^{40}$ Ar<sub>atm</sub> using the atmospheric ( $^{40}$ Ar/ $^{36}$ Ar)<sub>atm</sub> ratio of Lee et al. (2006). Uncertainty in the atmospheric ratio (298.56  $\pm$  0.31; Lee et al. 2006) is propagated through using a Monte Carlo method. The new <sup>40</sup>Ar<sub>atm</sub> determination is then subtracted from the total <sup>40</sup>Ar budget to determine the radiogenic component, <sup>40</sup>Ar\*. These steps are followed for both the unknown and the three neutron fluence monitors. In the study of Niespolo et al. (2017) the authors determine R-values (Eq. (7)) for Alder Creek sanidine sample relative to each of the neutron fluence monitors; Mes4, FCs, and A1. Here we redetermine these values with the incorporation of the  $^{39}$ K(n, $\alpha$ ,  $\beta$ )  $^{36}$ Ar interference. The R-value is a metric for the age relationship between any two samples (Renne et al. 1998) and is determined by:

$$R_{Y}^{X} = \frac{(e^{\lambda t_{X}} - 1)}{(e^{\lambda t_{Y}} - 1)} = \frac{(^{39}Ar^{*}/^{39}Ar_{K})_{X}}{(^{40}Ar^{*}/^{39}Ar_{K})_{Y}}$$
(7)

where  $\lambda$  is the total  ${}^{40}$ K decay constant, t is the age of the sample,  ${}^{40}$ Ar\* and <sup>39</sup>Ar<sub>K</sub> have the same definition as described previously, and X and Y are place holders for samples (e.g., X = ACs and Y = FCs). Modified Rvalues are determined for Alder Creek Sanidine to each neutron fluence monitor used in the Niespolo et al. (2017) study (supplement Table S2 and Fig. S6). The modified R-values are then combined with the astronomical ages of each neutron fluence monitor (Kuiper et al., 2008) and the total decay constant of (5.463  $\pm$  0.054)  $\times$  10<sup>-10</sup> a<sup>-1</sup> (Min et al., 2000). Model ages of 1.1847  $\pm$  0.0005 Ma, 1.1849  $\pm$  0.0005 Ma, and  $1.1870 \pm 0.0008$  Ma are calculated (for ages calibrated to Mes4, FCs, and A1; internal uncertainties only (Fig. 4A)). These result in a weighted mean of 1.1861  $\pm$  0.0006 Ma for the age including the  $^{39}$ K(n, $\alpha$ ,  $\beta$ ) $^{36}$ Ar inference which is greater than the weighted mean age of Niespolo et al. (2017) by approximately  $1.3 \pm 0.8$  ka. This bias in age is approximately equal to the 2  $\sigma$  analytical uncertainty of the study of Niespolo et al. (2017). We determine an  $\varepsilon(R_{\nu}^{X})$  value (Eq.8), which enables us to underline the change in the R-value that occurs when the interference from  $^{39}$ K(n, $\alpha$ ,  $\beta$ ) $^{36}$ Ar is taken into account, as compared to the R-value obtained when such interference is omitted. $\varepsilon(R_v^X)$  is calculated in an analogous fashion to epsilon notation commonly used in isotope geology

$$\varepsilon(R_{\gamma}^{X}) = \left( \left( \frac{R_{\gamma}^{X}incl}{R_{\gamma}^{X}omit} \right) - 1 \right) \times 10^{4}$$
(8)

where  $R_Y^{\rm X}incl$  and  $R_Y^{\rm X}omit$  are defined as the R-values determined with the inclusion and omission of the  $^{39}{\rm K}({\rm n},\alpha,\,\beta)^{36}{\rm Ar}$  interference, depicted in Fig. 4B.

We stress that the magnitude of the  $^{39}$ K(n, $\alpha$ ,  $\beta$ ) $^{36}$ Ar correction will be

dependent on the composition, atmospheric component, age, relationship between the unknown and the neutron fluence monitor, and  $\Delta t_{irr}$ . However, the uncertainty in both the  $^{40}K$  decay scheme and age of the monitor materials are still dominant in the complete uncertainty budget of an apparent  $^{40}\text{Ar}/^{39}\text{Ar}$  age. Nonetheless, the change in age determined is large enough to have implications for residence time studies (e. g., Rivera et al., 2013) and/or other applications requiring utmost precision. A generalized correction is shown in the next section.

# 4.3. General $^{39}K(n,\alpha,\beta)^{36}Ar$ correction and implications for $^{40}Ar/^{39}Ar$ geochronology

Here we present the  $^{39}\text{K}(n,\alpha)^{36}\text{Cl}$  inference correction and include the  $^{41}\text{K}(n,\alpha)^{38}\text{Cl}$  interference to make a direct comparison to previously documented chlorine corrections (Roddick, 1983; Foland et al., 1993; Renne et al., 2008). Like these previous studies we determine an initial production ratio (P( $^{36}\text{Cl}/^{38}\text{Cl})$ ), which is the ratio of  $^{36}\text{Cl}$  and  $^{38}\text{Cl}$  produced by  $(n,\gamma)$  reactions on  $^{35}\text{Cl}$  and  $^{37}\text{Cl}$ . This ratio is calculated from the irradiation simulation and then propagated through decay equations to determine a  $(^{36}\text{Ar}/^{38}\text{Ar})_{\text{K-Cl}}$ , for a given time since irradiation. Unlike these previous studies we also include the additional chlorine correction from  $^{36}\text{Cl}$  and  $^{38}\text{Cl}$  produced by the  $(n,\alpha)$  reactions on  $^{39}\text{K}$  and  $^{41}\text{K}$ .

A plot of the initial <sup>36</sup>Cl/<sup>38</sup>Cl ratio is shown in Fig. 5A for experimental values (Roddick, 1983; Foland et al. 1993; Renne et al. 2008) and modeled values of both Cl derived and K-derived chlorine corrections (Fig. S7 shows the cross-section for these interactions as a function of incident neutron energy). The disparity observed among these ratios can be attributed to two main factors. First, the utilization of difference reactors and shielding methods has a significant influence. For instance, Roddick (1983) and Foland et al. (1993) subjected their samples to irradiation without the use of cadmium shielding. Second, the inclusion or omission of different production channels during the determination process also contributes to this variation. Following Renne et al. (2008) the <sup>36</sup>Cl/<sup>38</sup>Cl ratio is converted to the <sup>36</sup>Ar/<sup>38</sup>Ar ratio through radiogenic ingrowth equations. In Fig. 5B, we present the  $(^{36}Ar/^{38}Ar)_{Cl}$  ratio as a function of time since irradiation ( $\Delta t_{irr}$ ) for the experimental data (Roddick, 1983; Foland et al., 1993; Renne et al., 2008) and modeled production ratios for both Cl- and K- derived chlorine corrections. The respective model production ratios are calculated to be 238.8  $\pm$  6.2 for Cl-derived and 475  $\pm$  112 for K-derived corrections, with the combined value (242.0  $\pm$  6.5) displayed in Fig. S8. These ratios are determined from the simulated irradiation by counting the produced isotopes and errors are derived from Poisson statistics. Relative production rates for  $^{36}$ Ar and  $^{38}$ Ar by both the Cl-derived  $(n,\gamma)$  and K-derived  $(n,\alpha)$  pathways are shown in Fig. S9. We caution the use of <sup>38</sup>Ar as a direct tracer for Cl without correction for the <sup>38</sup>Ar production from <sup>41</sup>K, however the dominance of the cross-section in the thermal energy region of the  $(n,\gamma)$ reactions on Cl mean that these reactions dominate the production budget by ~46 and 4.5 times compared to the  $(n,\alpha)$  reactions on K for <sup>36</sup>Ar and <sup>38</sup>Ar production respectively (Fig. S9). Nonetheless, the absolute necessity of measuring potassium means the  $(n,\alpha)$  reaction corrections are applicable to all analyzed samples and neutron fluence

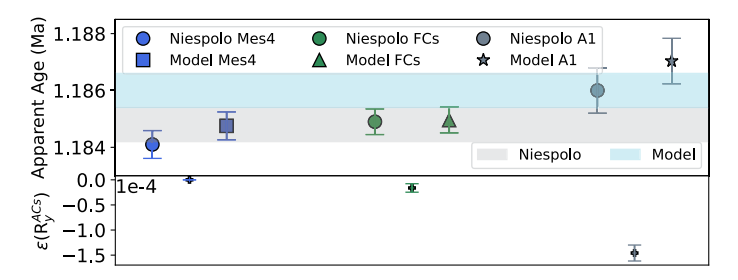


Fig. 4. Re-determination of the age of Alder Creek sanidine with the inclusion of the  $^{39}$ K(n, $\alpha,\beta$ ) $^{36}$ Ar nuclear channel included in the relationship value of R for Alder Creek with each neutron fluence monitor. Horizontal bars in the top panel show the weighted mean age and uncertainty of Niespolo et al. (2017) (gray) and the model determined age (skyblue). The bottom panel shows  $\varepsilon(R_x^y)$  with uncertainties determined by a Monte Carlo sampling at plotted at the  $1\sigma$  level.

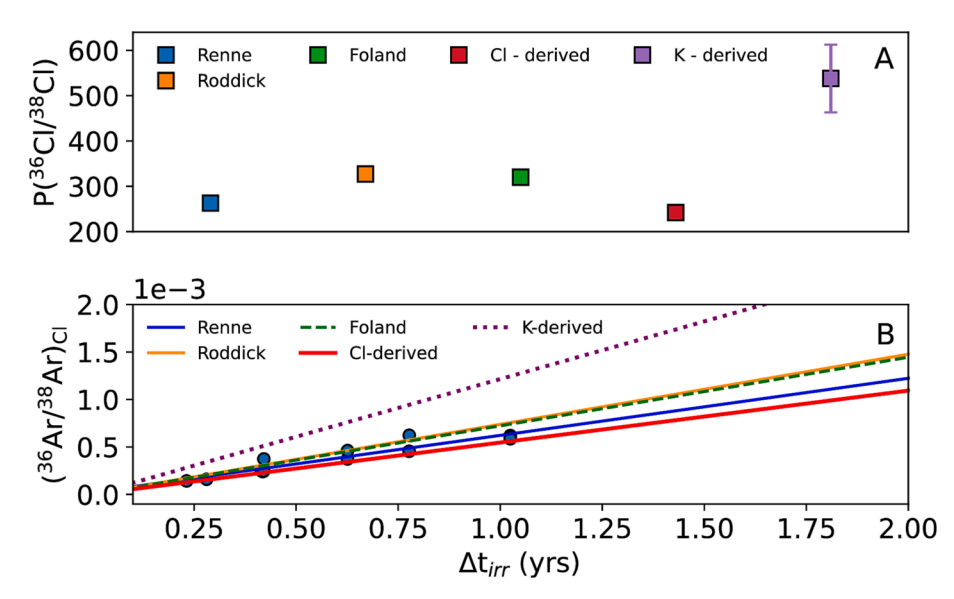


Fig. 5. Panel A shows experimental values of P (<sup>36</sup>Cl/<sup>38</sup>Cl) (Roddick, 1983; Foland et al. 1993; Renne et al. 2008) and model values for P(36Cl/38Cl) determined by nuclear channels from Cl and K. Error bars are 1 and are shown where they have been documented but are smaller than the marker size. Panel B shows data from Renne et al., (2008) (blue circles) which measured the  ${}^{36}Ar_{Cl}/{}^{38}Ar_{Cl}$  ratio in neutronirradiated NaCl at various times after irradiation and the best fitting line to these data is shown in blue. Calculated curves are also plotted for 36Cl/38Cl of ~252, 320, 327, 238, and 475 which correspond to determined values from Renne et al. (2008). Roddick (1983), Foland et al. (1993), and the model determined production ratio for chlorine corrections derived from Cl and K isotopes.

monitors.

To determine how an apparent  $^{40}{\rm Ar}/^{39}{\rm Ar}$  age will be affected by the inclusion of the  $^{39}{\rm K}(n,\alpha,\beta)^{36}{\rm Ar}$  inference we use a Monte Carlo simulation to propagate a  $(^{36}{\rm Ar}/^{39}{\rm Ar})_{\rm K}$  ratio for a reasonable  $\Delta$   $t_{irr}$  (ca. 3–12 months). Corrected age normalized to uncorrected age as a function of  $\Delta$   $t_{irr}$  is shown in Fig. 6. For a typical  $\Delta$   $t_{irr}$ , the corrected age will be approximately 0.05–0.4% older than determined with this interference omitted.

# 4.4. K-derived <sup>36</sup>Ar correction dependence

Like the K-derived  $^{40}$ Ar correction, the magnitude of the K-derived  $^{36}$ Ar correction is a direct function of the neutron fluence, inverse to the

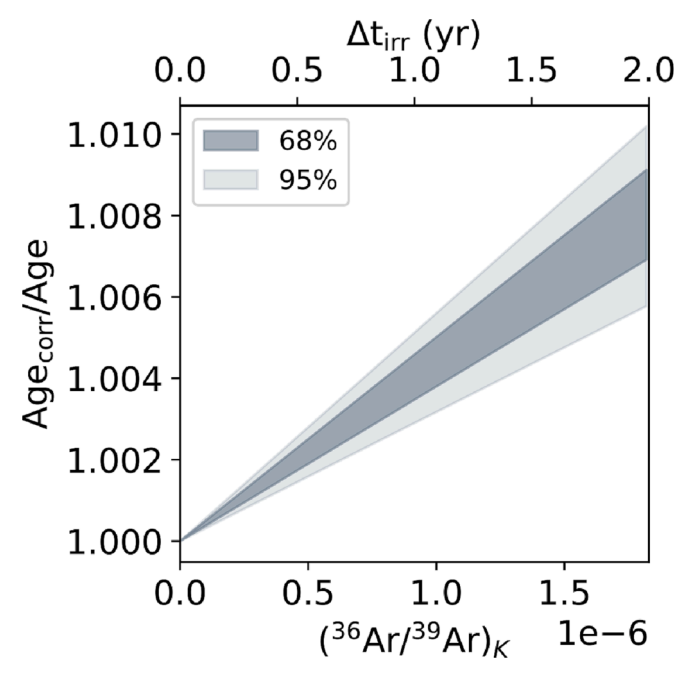


**Fig. 6.** Effect on apparent age including the  $^{39}$ K(n, $\alpha$ ,  $\beta$ ) $^{36}$ Ar inference (Age<sub>corr</sub>) normalized to the uncorrected age (production channel omitted). All other parameters of the age calculation remained constant such that the change in age is only by the inclusion or omission of this production channel. Age change for a typical  $\Delta t_{irr}$  (~3–6 months) is approximately 0.2  $\pm$  0.05%. 68% and 95% credible intervals shown as shades of darker and lighter shades of gray.

age and is independent of the K/Ca of the sample (e.g., Dalrymple, 1981). As a result of these dependences the magnitude and direction (older/younger) of the change in age will hinge on the relationship between the neutron fluence monitor and the unknown. We explore this by determining the change in the unknown age including the <sup>39</sup>K  $(n,\alpha,\beta)^{36}$ Ar inference relative to the identically corrected commonly used neutron fluence monitors: (1) Alder Creek sanidine (ACs; Niespolo et al., 2017); (2) Fish Canvon sanidine (FCs; Kuiper et al., 2008); (3) GA1550 Biotite (GA1550; McDougall and Wellman, 2011), and; (4) Hb3gr hornblende (Hb3gr; Jourdan et al., 2006). To make these age corrections we use corrected R values  $R_S^U$ , where U and S define the  $^{40}\text{Ar*}/^{39}\text{Ar}_K$  ratios of the unknown and neutron fluence monitor. R values are then corrected for by including the  $^{39}$ K(n, $\alpha$ , $\beta$ ) $^{36}$ Ar interference and are propagated through a range of unknown ages spanning ca. 0-4600 Ma against each of the aforementioned fluence monitors. We assume that the analysis of the unknown and neutron fluence monitor occur at the same time, the production of <sup>39</sup>Ar<sub>K</sub> is the same for the unknown and neutron fluence monitor,  $\Delta t_{irr}$  is 1 year. Also assumed is that each neutron fluence monitor and unknown have a consistent  $^{40}\text{Ar*}/^{40}\text{Ar}_{atm}$  (ratio of radiogenic  $^{40}\text{Ar}$  too atmospheric  $^{40}\text{Ar}$ ) which is likely unphysical but we are using Fig. 7 to illustrate the main implications when the  $^{39}$ K $(n,\alpha,\beta)^{36}$ Ar interference is included. The key insights derived from this are twofold. First, the alteration in age hinges on the relationship between the unknown sample and the neutron fluence monitor. When the unknown sample is younger than the neutron fluence monitor, incorporating this correction will lead to the calculated ages of the unknown appearing older. Conversely, if the unknown sample is older than the neutron fluence monitor, accounting for this interference will yield younger calculated ages for the unknown sample. Second, the extent of the age change is directly linked to the magnitude of the age difference between the unknown sample and the neutron fluence monitor. An extreme example of this is when a young sample, less than 1 Ma, is calibrated using the 1073.6 Ma old Hg3br neutron fluence monitor. This would result in an approximate 0.5% increase in the calculated age of the sample, as illustrated in Fig. 7.

Fig. 7 highlights the principal conclusions and controlling parameters of this interference correction. However, we have shown in the example using the raw data of Niespolo et al. (2017) that the  $^{39}\text{K}$  (n, $\alpha,\beta)^{36}\text{Ar}$  interference correction will be unique to the particular unknown and neutron fluence monitor(s) used and should be determined using the measured  $^{39}\text{Ar}_K$  through the ( $^{36}\text{Ar}/^{39}\text{Ar}_K$  ratio given in Eq. (6). We give the interference equations for all Ar nuclei with this production channel in the supplement. These simulations reiterate the cautions of

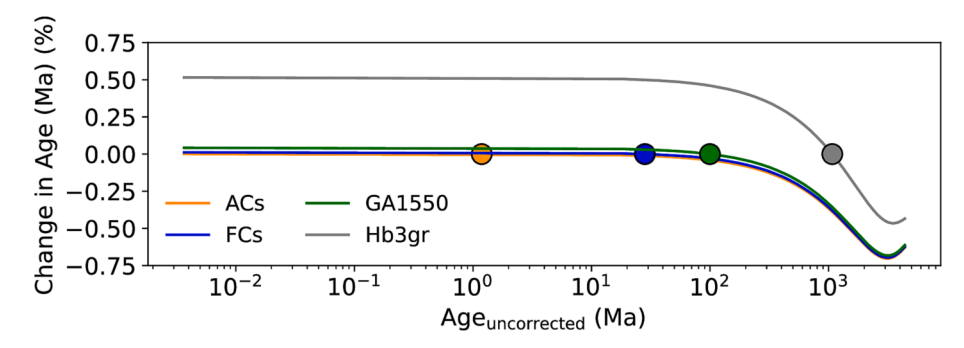


**Fig. 7.** Effect of  $^{39}$ K(n, $\sigma$ , $\beta$ ) $^{36}$ Ar interference on unknown ages relative to commonly used neutron fluence monitors: ACs; FCs; GA1550 and; Hb3gr. Dots on this plot indicate the position at which the unknown and neutron fluence monitor are the same age at which point the  $^{39}$ K(n, $\sigma$ , $\beta$ ) $^{36}$ Ar interference correction cancels and there is no change in age.

Renne et al. (2008) that long irradiations and lengthy delay between irradiation and analysis can produce significant age errors in all samples due to both  $(n,\gamma)$  reactions on  $^{35}$ Cl and  $^{37}$ Cl (Renne et al. 2008) and  $(n,\alpha)$  chlorine producing reactions on  $^{39}$ K and  $^{41}$ K.

In the next section we validate the simulations completed in this study and for this correction by modeling the irradiation of pure potassium salt (KCl) and then comparing modeled interference ratios to experimental measurements by Renne et al. (2005).

# 4.5. Salt irradiation

The irradiation of pure salts, such as  $CaF_2$  and KCl, are used to determine the relative production ratio of Ar on isotopes of Ca and K to make interference corrections. To validate the simulations of this study and quantify the various interferences on potassium we perform simulated irradiation of KCl salt using GEANT4. Simulated production ratios are then compared with literature values for the CLICIT facility of the TRIGA reactor at OSTR (Renne et al. 2005). Simulated and experimentally determined interferences are shown in Table 2. Cross-section for the major production pathways are shown in supplementary Fig. S10 with the simulated inference ratios shown and compared to data in Fig. S11.

We find that the simulated interference ratios are largely consistent with the experimental determinations of Renne et al. (2005). The results shown mainly minor discrepancies however, the simulated  $(^{38}\text{Ar}/^{39}\text{Ar})_K$  ratio is approximately 30% greater than the experimentally determined value, we explore plausible explanations in the discussion section. These inference corrections and the general concordance with the data of Renne et al. (2005) verify that the model does a reasonable job of simulating the irradiation conditions of the CLICIT facility and that the  $^{39}\text{K}(n,\alpha,\beta)^{36}\text{Ar}$  nuclear channel should be included in future analytical protocols.

Table 2 Nuclear channels for the production of Ar and Cl from K isotopes. All uncertainties  $1\sigma$ .

Production ratio	Fission-spectrum neutrons (Cd-shielded) <sup>1</sup>	Simulation*
(40 Ar/39 Ar) <sub>K</sub>	$(7.30 \pm 0.92) \times 10^{-4}$	$(7.9 \pm 1.9) \times 10^{-4}$
(38 Ar/39 Ar) <sub>K</sub>	$(1.22 \pm 0.00) \times 10^{-2}$	$(1.6 \pm 0.08) \times 10^{-2}$
(37 Ar/39 Ar) <sub>K</sub>	$(2.24 \pm 0.16) \times 10^{-4}$	N/A
(36 Cl/39 Ar) <sub>K</sub>	N/A	$(0.40 \pm 0.01) \times 10^{-1}$
(41 Ar/39 Ar) <sub>K</sub>	N/A	$(2.15 \pm 0.05) \times 10^{-3}$
(36 Ar/38 Ar) <sub>Cl</sub>	257.8 ± 2.5	$239 \pm 6$
(36 Ar/38 Ar) <sub>Cl</sub>	N/A	447 + 106

<sup>\*</sup> This study.

# 5. Discussion

# 5.1. Implications of the additional interferences

The inclusion of the  $^{39}$ K(n, $\alpha$ , $\beta$ ) $^{36}$ Ar interference will affect all absolute  $^{40}$ Ar/ $^{39}$ Ar ages. Although this change in age is slight (Fig. 6) there are potential implications for high precision studies, where the modification in age with the inclusion of this interference is at the level of the analytical precision of the measurement, such as dating of mass extinction events (e.g., Renne et al. 2015; Sprain et al., 2015), or the reevaluation of the ages of neutron fluence monitors (e.g., Kuiper et al., 2008; Niespolo et al., 2017). The effect of including the  $^{39}$ K(n, $\alpha$ , $\beta$ ) $^{36}$ Ar interference becomes more pronounced with: (1) An increase in time between irradiation and analysis ( $\Delta$ t<sub>irr</sub>) (Fig. 7) and; (2) Larger differences between the age of the unknown sample and the neutron fluence monitor age (Fig. 7). This underscores that minimizing  $\Delta$ t<sub>irr</sub> (observing precautions for safe handling) and matching the ages of the unknown sample and neutron fluence monitor are the best practices in  $^{40}$ Ar/ $^{39}$ Ar dating.

Additionally, the use of  $^{38}$ Ar as a means to determine cosmogenic exposure ages (e.g., Shuster and Cassata, 2015) or as a chemical tracer for Cl (e.g., Kelley et al., 1986) could be affected by the overlooked  $^{41}$ K  $(n,\alpha,\beta)^{38}$ Ar interference.

# 5.2. Nuclear cross sections

All GEANT4 simulations shown in this paper require the use of physics databases for the nuclear cross-sections as a function of the incident neutron energy. Fig. 1 shows the nuclear database cross-section (ENDF VIII.0 database) with recent measurements of the cross-section by Rutte et al., (2019) using D-D fusion neutrons and  $^7\text{Li}(p,n)^7\text{B}$  of the  $^{39}\text{K}(n,p)^{39}\text{Ar}$  nuclear channel. It is evident from the measurements of Rutte et al., (2019) that there is additional structure in the cross sections across the 1–3 MeV range with a resonance peak at ca. 2.5 MeV. As well as the excess structure for the  $^{39}\text{K}(n,p)^{39}\text{Ar}$  reaction, it is plausible that other important reaction channels on K isotopes may have more complex structure unaccounted for in these physics databases. Additional resonances for isotopes with similar atomic number nuclei such as chlorine, have also been observed using the same D-D fusion neutron source as Rutte et al. (2019), as documented by Batchelder et al. (2019).

In the K-salts irradiation example the discrepancies between the simulated and measured interferences may be explained in two ways; (1) A different neutron energy spectrum between the simulation and that experienced by the sample in the CLICIT facility at the OSTR reactor and; (2) Unaccounted for excess structure in the simulations relative to the most recent measurements (Rutte et al., 2019). It is likely that the differences between these values are a combination of both factors which we outline next. We see concordance for  $(^{40}\text{Ar}/^{39}\text{Ar})_K$  suggesting that the neutron fluence is adequately described in the thermal energy

<sup>&</sup>lt;sup>1</sup> Renne et al., (2005).

region where this reaction is dominant; however, the  $(^{38}Ar/^{39}Ar)_{K}$  is about 30% greater for the simulated value. The production of <sup>38</sup>Ar by the <sup>39</sup>K(n,np)<sup>38</sup>Ar nuclear channel is dominant in the higher energy region (sharp peak in the cross-section greater than 7 MeV; supplement Fig. S10) which suggests that the neutron fission spectrum of the simulations is subtly different in the higher energy regime. This will require addressing in further model iterations. The other potential reason for slight differences between model and data is in the underlying physics cross-section databases. GEANT4 simulations require reaction crosssection data to be included in each simulation. The ENDF crosssections (Brown et al. 2018) used in these simulations are smooth and do not account for the recently measured additional structure in the cross-section of the <sup>39</sup>K(n,p)<sup>39</sup>Ar reaction (Rutte et al., 2019). Given that these ratios are dependent on these nuclear channel cross-sections integrated over the incident neutron energies, the variation in the interference ratios would need to be of the same order of magnitude as the variation in the cross-section to explain the discrepancy (i.e.,  $\sim$ 30%). Rutte et al. (2019) showed that in the 1-3 MeV there were additional resonances in the cross-section of the  $^{39}$ K(n,p)  $^{39}$ Ar that are  $\sim$ 5 times larger than the ENDF database (Brown et al., 2018). Therefore, it is plausible that this is also a factor in the difference between simulated ratios and the suite of data, especially in the higher energy region (>1 MeV). We can do an additional check using the chlorine production ratio from <sup>35</sup>Cl and <sup>37</sup>Cl, P(<sup>36</sup>Ar/<sup>38</sup>Ar)<sub>Cl</sub>, which is independent of the known additional structure in the <sup>39</sup>K(n,p) <sup>39</sup>Ar cross-section and spans the entire fission neutron energy regime. The measured value from Renne et al. (2008) is 258  $\pm$  2.5 and the simulated value is 239  $\pm$  6. The lesser difference (~8%) between these two values relative to the ( $^{38}$ Ar/ $^{39}$ Ar)<sub>K</sub> variation suggests that it is likely a combination of a subtly different neutron energy spectrum and additional unaccounted for structure in the cross-section of argon producing nuclear channels on potassium isotopes.

# 6. Conclusion

In this work we have presented simulations of neutron irradiation for routinely measured materials used for interference corrections in  $^{40}\mathrm{Ar}/^{39}\mathrm{Ar}$  geochronology. We document the secondary nuclei and particles that are formed during the irradiation of routinely analyzed samples which highlights the complexity of the irradiation process and potential mass spectrometry interferences by introducing hydrocarbons and helium/hydrogen into the system.

Furthermore, simulations of a feldspar type sample has highlighted a previously overlooked production pathway of  $^{36}\text{Ar}$  from  $^{39}\text{K}$  by the  $^{39}\text{K}$  (n,a, $\beta)^{36}\text{Ar}$  nuclear channel. The inclusion of this inference results in apparent ages that are older by ca. 0.05–0.4% for typical elapsed time since the irradiation ( $\Delta t_{irr}=3\text{-}6$  months). However, this change in age is illustrative and will be unique to the suite of the sample to be analyzed, irradiation protocol and relationship between the unknown and neutron fluence monitor used. The interference correction should be determined by the  $(^{36}\text{Ar}/^{39}\text{Ar})_K$  ratio and the known  $\Delta t_{irr}$  (Fig. 6B). This interference should be incorporated into routine data analysis, and may be especially important in the intercalibration of the  $^{40}\text{Ar}/^{39}\text{Ar}$  system with other chronometers (e.g.,  $^{206}\text{Pb}/^{238}\text{U}$ ).

However, we reiterate EARTHTIME goals (Bowring et al. 2005) that further refinements of neutron fluence monitor ages and determination of the  $^{40}$ K decay constant are needed to put this overlooked interference into more meaningful context.

The modeling presented here may also provide the first step in a complete simulation of a sample from formation to data acquisition allowing complex multi-phase geologic histories to be combined with potential isotopic disturbance of the irradiation process to be interrogated.

These simulations are validated by comparison of interference correction for K-salts. We show relative concordance with these values to those measured but also highlight the need for more physical measurements for the K cross-sections for Ar producing nuclear channels. These may also be of importance to the nuclear physics community, e.g., for nuclear salt reactors using fuels which contain potassium.

# **Declaration of Competing Interest**

The authors declare the following financial interests/personal relationships which may be considered as potential competing interests: 'The authors declare that they have no known competing financial interest or personal interest that could interfere with the work presented here. Any use of trade, firm, or product names is for descriptive purposes only and does not imply endorsement by the U.S. Government.'.

# Acknowledgements

We acknowledge funding support from National Science Foundation grant EAR2102788 and the Ann and Gordon Getty Foundation.

### Research data

Research data has been supplied via a repository: https://github.com/jcarter-1/Nucleogenic 36Ar and 10.6084/m9.figshare.22126607.

# Appendix A. Supplementary material

Supplementary material with additional data, simulations, and the suite of  $^{40}$ Ar/ $^{39}$ Ar correction equations can be found online at htt ps://doi.org/10.1016/j.gca.2023.07.017.

### References

- Agostinelli, S., Allison, J., Amako, K.A., Apostolakis, J., Araujo, H., Arce, P., Asai, M., Axen, D., Banerjee, S., Barrand, G.J.N.I., Behner, F., 2003. GEANT4—a simulation toolkit. Nucl. Instrum. Methods Phys. Res., Sect. A 506 (3), 250–303.
- Batchelder, J.C., Chong, S.A., Morrell, J., Unzueta, M.A., Adams, P., Bauer, J.D., Bailey, T., Becker, T.A., Bernstein, L.A., Fratoni, M., Hurst, A.M., 2019. Possible evidence of nonstatistical properties in the <sup>36</sup>Cl(n, p) <sup>36</sup>S cross section. Phys. Rev. C 99 (4), 044612.
- Bowring, S.A., Erwin, D., Parrish, R., Renne, P.R., 2005. EARTHTIME: A community-based effort towards high-precision calibration of earth history. Geochim. Cosmochim. Acta. 69, A316–A.
- Brereton, N.R., 1970. Corrections for interfering isotopes in the  $^{40}$ Ar/ $^{39}$ Ar dating method. Earth Planet. Sci. Lett 8 (6), 427–433.
- Brown, D.A., Chadwick, M.B., Capote, R., Kahler, A.C., Trkov, A., Herman, M.W., Sonzogni, A.A., Danon, Y., Carlson, A.D., Dunn, M., Smith, D.L., 2018. ENDF/B-VIII.0: The 8th major release of the nuclear reaction data library with CIELO-project cross sections, new standards and thermal scattering data. Nucl. Data Sheets 148, 1, 142
- Clauer, N., Zwingmann, H., Liewig, N., Wendling, R., et al., 2012. Comparative <sup>40</sup>Ar/<sup>39</sup>Ar and K-Ar dating of illite-type clay minerals: A tentative explanation for age identities and differences. Earth Sci. Rev. 115 (1–2), 76–96.
- Dalrymple, G.B., 1981. Irradiation of samples for <sup>40</sup>Ar/<sup>39</sup>Ar dating using the Geological Survey TRIGA reactor. Geol. Surv. Prof. Pap. 1176, 1–55.
   Dalrymple, G.B., Lanphere, M.A., 1971. <sup>40</sup>Ar/<sup>39</sup>Ar technique of K/Ar dating: a
- Dalrymple, G.B., Lanphere, M.A., 1971. "VAr/3" Ar technique of K/Ar dating: a comparison with the conventional technique. Earth Planet. Sci. Lett 12 (3), 300–308.
- Foland, K.A., Fleming, T.H., Heimann, A., Elliot, D.H., 1993. Potassium-argon dating of fine-grained basalts with massive Ar loss: Application of the 40Ar/39Ar technique to plagioclase and glass from the Kirkpatrick Basalt, Antarctica. Chem. Geol. 107 (1–2), 173–190.
- Hall, C.M., 2014. Direct measurement of recoil effects on <sup>40</sup>Ar/<sup>39</sup>Ar standards. Geol. Soc., Lond., Special Publ. 378 (1), 53–62.
- Hariasz, L., Stukel, M., Di Stefano, P.C.F., Rasco, B.C., Rykaczewski, K.P., Brewer, N.T., Stracener, D.W., Liu, Y., Gai, Z., Rouleau, C., Carter, J., 2022. First observation of the ground-state electron-capture of <sup>40</sup>K. arXiv preprint arXiv:2211.10343.
- Jourdan, F., Verati, C., Féraud, G., 2006. Intercalibration of the Hb3gr <sup>40</sup>Ar/<sup>39</sup>Ar dating standard. Chem. Geol. 231 (3), 177–189.
  Jourdan, F., Matzel, J.P., Renne, P.R., 2007. <sup>39</sup>Ar and <sup>37</sup>Ar recoil loss during neutron
- Jourdan, F., Matzel, J.P., Renne, P.R., 2007. <sup>39</sup>Ar and <sup>37</sup>Ar recoil loss during neutron irradiation of sanidine and plagioclase. Geochim. Cosmochim. Acta 71 (11), 2791–2808.
- Kelley, S., Turner, G., Butterfield, A., Shepherd, T.J., 1986. The source and significance of argon isotopes in fluid inclusions from areas of mineralization. Earth Planet. Sci. Lett 79 (3–4), 303–318.
- Kuiper, K.F., Hilgen, F.J., Steenbrink, J., Wijbrans, J.R., 2004. <sup>40</sup>Ar/<sup>39</sup>Ar ages of tephras intercalated in astronomically tuned Neogene sedimentary sequences in the eastern Mediterranean. Earth Planet. Sci. Lett. 222 (2), 583–597.
- Kuiper, K.F., Deino, A., Hilgen, F.J., Krijgsman, W., Renne, P.R., Wijbrans, A.J., 2008. Synchronizing rock clocks of Earth history. science 320 (5875), 500–504.

- Lee, J.Y., Marti, K., Severinghaus, J.P., Kawamura, K., Yoo, H.S., Lee, J.B., Kim, J.S., 2006. A redetermination of the isotopic abundances of atmospheric Ar. Geochim. Cosmochim. Acta 70 (17), 4507–4512.
- McDougall, I., Harrison, T.M., 1999. Geochronology and Thermochronology by the  $^{40}{\rm Ar}/^{39}{\rm Ar}$  Method. Oxford University Press on Demand.
- McDougall, I., Roksandic, Z., 1974. Total fusion 40Ar/39Ar ages using HIFAR reactor. J. Geol. Soc. Austr. 21 (1), 81–89.
- McDougall, I., Wellman, P., 2011. Calibration of GA1550 biotite standard for K/Ar and  $^{40}$ Ar/ $^{39}$ Ar dating. Chem. Geol. 280 (1–2), 19–25.
- Merrihue, C., Turner, G., 1966. Potassium-argon dating by activation with fast neutrons. J. Geophys. Res. 71 (11), 2852–2857.
- Min, K., Mundil, R., Renne, P.R., Ludwig, K.R., 2000. A test for systematic errors in 40Ar/39Ar geochronology through comparison with U/Pb analysis of a 1.1-Ga rhyolite. Geochim. Cosmochim. Acta. 64 (1), 73–98.
- Mitchell, J.G., 1968. The <sup>40</sup>Ar/<sup>39</sup>Ar method for potassium-argon age determination. Geochim. Cosmochim. Acta 32 (7), 781–790.
- Mixon, E.E., Jicha, B.R., Tootell, D., Singer, B.S., 2022. Optimizing 40Ar/39Ar analyses using an Isotopx NGX-600 mass spectrometer. Chem. Geol. 593, 120753.
- Niespolo, E.M., Rutte, D., Deino, A.L., Renne, P.R., 2017. Intercalibration and age of the Alder Creek sanidine <sup>40</sup>Ar/<sup>39</sup>Ar standard. Quat. Geochronol. 39, 205–213.
- Onstott, T.C., Miller, M.L., Ewing, R.C., Arnold, G.W., Walsh, D.S., 1995. Recoil refinements: Implications for the <sup>40</sup>Ar/<sup>39</sup>Ar dating technique. Geochim. Cosmochim. Acta 59 (9), 1821–1834.
- Paine, J.H., Nomade, S., Renne, P.R., 2006. Quantification of <sup>39</sup>Ar recoil ejection from GA1550 biotite during neutron irradiation as a function of grain dimensions. Geochim. Cosmochim. Acta. 70 (6), 1507–1517.
- Phillips, D., Matchan, E.L., 2013. Ultra-high precision <sup>40</sup>Ar/<sup>39</sup>Ar ages for Fish Canyon Tuff and Alder Creek Rhyolite sanidine: new dating standards required? Geochim. Cosmochim. Acta 121, 229–239.
- Phillips, D., Matchan, E.L., Honda, M., Kuiper, K.F., 2017. Astronomical calibration of <sup>40</sup>Ar/<sup>39</sup>Ar reference minerals using high-precision, multi-collector (ARGUSVI) mass spectrometry. Geochim. Cosmochim. Acta 196, 351–369.
- Renne, P.R., Swisher, C.C., Deino, A.L., Karner, D.B., Owens, T.L., DePaolo, D.J., 1998. Intercalibration of standards, absolute ages and uncertainties in <sup>40</sup>Ar/<sup>39</sup>Ar dating. Chem. Geol. 145 (1–2), 117–152.
- Renne, P.R., Knight, K.B., Nomade, S., Leung, K.N., Lou, T.P., 2005. Application of deuteron-deuteron (D–D) fusion neutrons to <sup>40</sup>Ar/<sup>39</sup>Ar geochronology. Appl. Radiat. Isot. 62 (1), 25–32.
- Renne, P.R., Sharp, Z.D., Heizler, M.T., 2008. Cl-derived argon isotope production in the CLICIT facility of OSTR reactor and the effects of the Cl-correction in <sup>40</sup>Ar/<sup>39</sup>Ar geochronology. Chem. Geol. 255 (3–4), 463–466.
- Renne, P.R., Mundil, R., Balco, G., Min, K., Ludwig, K.R., 2010. Joint determination of <sup>40</sup>K decay constants and <sup>40</sup>Ar\*, <sup>40</sup>K for the Fish Canyon sanidine standard, and

- improved accuracy for  $^{40}{\rm Ar}/^{39}{\rm Ar}$  geochronology. Geochim. Cosmochim. Acta 74 (18), 5349–5367.
- Renne, P.R., Sprain, C.J., Richards, M.A., Self, S., Vanderkluysen, L., Pande, K., 2015. State shift in Deccan volcanism at the Cretaceous-Paleogene boundary, possibly induced by impact. Science 350 (6256), 76–78.
- Rivera, T.A., Storey, M., Zeeden, C., Hilgen, F.J., Kuiper, K., 2011. A refined astronomically calibrated 40Ar/39Ar age for Fish Canyon sanidine. EPSL 311 (3–4), 420–426.
- Rivera, T.A., Storey, M., Schmitz, M.D., Crowley, J.L., 2013. Age intercalibration of <sup>40</sup>Ar/<sup>39</sup>Ar sanidine and chemically distinct U/Pb zircon populations from the Alder Creek Rhyolite Quaternary geochronology standard. Chem. Geol. 345, 87–98.
- Roddick, J.C., 1983. High precision intercalibration of <sup>40</sup>Ar/<sup>39</sup>Ar standards. Geochim. Cosmochim. Acta 47 (5), 887–898.
- Rutte, D., Pfänder, J.A., Koleška, M., Jonckheere, R., Unterricker, S., 2015. Radial fastneutron fluence gradients during rotating <sup>40</sup>Ar/<sup>39</sup>Ar sample irradiation recorded with metallic fluence monitors and geological age standards. Geochem. Geophys. 16 (1), 336–345.
- Rutte, D., Becker, T.A., Deino, A.L., Reese, S.R., Renne, P.R., Schickler, R.A., 2018. The new CLOCIT irradiation facility for <sup>40</sup>Ar/<sup>39</sup>Ar geochronology: Characterisation, comparison with CLICIT and implications for high-precision geochronology. Geostandard. Geoanal. Res. 42 (3), 301–307.
- Rutte, D., Renne, P.R., Morrell, J., Qi, L., Ayllon, M., van Bibber, K., Wilson, J., Becker, T. A., Batchelder, J., Bernstein, L.A., Lebois, M., 2019. Boutique neutrons advance <sup>40</sup>Ar/<sup>39</sup>Ar geochronology. Sci. Adv. 5 (9), p.eaaw5526.
- Shuster, D.L., Cassata, W.S., 2015. Paleotemperatures at the lunar surfaces from open system behavior of cosmogenic <sup>38</sup>Ar and radiogenic <sup>40</sup>Ar. Geochim. Cosmochim. Acta 155, 154–171.
- Sprain, C.J., Renne, P.R., Wilson, G.P., Clemens, W.A., 2015. High-resolution chronostratigraphy of the terrestrial Cretaceous-Paleogene transition and recovery interval in the Hell Creek region, Montana. *Bulletin* 127 (3–4), 393–409.
- Stukel, M., Hariasz, L., Di Stefano, P.C.F., Rasco, B.C., Rykaczewski, K.P., Brewer, N.T., Stracener, D.W., Liu, Y., Gai, Z., Rouleau, C., Carter, J., 2022. Rare <sup>40</sup>K decay with implications for fundamental physics and geochronology. arXiv preprint arXiv: 2211.10319.
- Tetley, N., McDougall, I., Heydegger, H.R., 1980. Thermal neutron interferences in the  $^{40}$ Ar/ $^{39}$ Ar dating technique. J. Geophys. Res: Solid Earth 85 (B12), 7201–7205.
- Turner, G., 1971. Argon 40-argon 39 dating: The optimization of irradiation parameters. Earth Planet, Sci. Lett 10 (2), 227–234.
- Turner, G., Cadogan, P.H., 1974. Possible effects of <sup>39</sup>Ar recoil in <sup>40</sup>Ar/<sup>39</sup>Ar dating. In: Lunar and Planetary Science Conference Proceedings, vol. 5, pp. 1601–1615.
- Villa, I.M., 1997. Direct determination of <sup>39</sup>Ar recoil distance. Geochim. Cosmochim. Acta 61 (3), 689–691.
- Watt, B.E., 1952. Energy spectrum of neutrons from thermal fission of <sup>235</sup>U. Phys. Rev. 87 (6), 1037.